Robust Design for STAR-RIS Secured Internet of Medical Things

Wen Wang*, Wanli Ni*, Hui Tian*, Zhaohui Yang†, Chongwen Huang‡, and Kai-Kit Wong†
*State Key Lab. of Networking and Switching Technology, Beijing Univ. of Posts and Te lecommun., Beijing, China
†Department of Electronic and Electrical Engineering, University College London, London, UK
‡Zhejiang Provincial Key Laboratory of Info. Proc., Commun. & Netw., Zhejiang University, Hangzhou, China
Email: {wen.wang,charleswall,tianhui}@bupt.edu.cn; {yang.zhaohui,kai-kit.wong}@ucl.ac.uk; chongwenhuang@zju.edu.cn

***Abstract*—This paper investigates the secure and efficient e-health data transmission problem in a simultaneously transmitting and reflecting (STAR) reconfigurable intelligent surface (RIS) assisted Internet of Medical Things (IoMT) network. The STAR-RIS is employed to safeguard the patients' telemedicine against eavesdroppers in the whole space. The joint active and passive beamforming is developed to maximize the secrecy energy efficiency (SEE), taking into account the imperfect channel state information (CSI) of all channels. By approximating the semi-infinite inequality constraints with $\mathcal{S}$-procedure and general sign-definiteness, the reformulated problem is solved by an alternating optimization framework. Simulation results reveal that: 1) STAR-RIS can achieve more noteworthy SEE gain for IoMT networks than conventional reflecting-only RIS; 2) The equal time splitting mode of STAR-RIS is preferable for low power domain, while the energy splitting mode achieves the best performance when the downlink power is sufficient; 3) The accuracy of CSI estimation and the bit resolution power consumption are crucial to reap the SEE benefits offered by STAR-RIS.**

***Index Terms*—Internet of Medical Things, reconfigurable intelligent surface, robust beamforming, secure communication.**

I. Introduction

Internet of Medical Things (IoMT) networks enable remote monitoring and diagnosis of the homebound patients by using wireless communication technologies to transmit telemedicine data [1]. Spurred by economic and privacy concerns, energy efficiency and information security are of crucial importance for IoMT networks. The existing security techniques for IoMT networks mainly rely on application layer and transport layer encryption. For instance, the authors of [2] considered using the datagram transport layer security protocol to satisfy data confidentiality and privacy requirements, while the constrained application protocol and transport layer security version 1.3 were suggested in [3]. However, since decryption involves solving mathematical problems, these encryption protocols will be compromised to adversaries with powerful calculating ability. To this end, physical layer security (PLS), as a complement to higher-layer encryption techniques, may hold the key to offer reliable and efficient medical responses.

Owing to its capability of modifying the propagation environment, reconfigurable intelligent surface (RIS) is particularly appealing in various PLS technologies [4]. Specifically, the RIS consisting of low-cost passive elements can work stably without dedicated energy supply. With the aid of a software-programmable controller connected to the RIS, the signals from different paths can be coherently combined at the legitimate receivers to enhance the desired signal, or destructively at the malicious eavesdroppers (Eves) to avoid information leakage. Enlightened by the benefits of integrating RISs into secure and energy efficient communication, RIS-assisted communications have attracted increasing attention [4]–[6]. The adoption of RISs for energy saving was envisioned and its realistic power consumption model was developed in [4]. The authors of [5] presented a power-efficient scheme to minimize the transmit power subject to the secrecy constraint. Moreover, assuming imperfect channel state information (CSI) of Eves, an energy efficiency maximization problem was studied in [6]. However, these researches assume that RISs can only serve the transmitters and receivers located at the same side. Obviously, this geographical constraint gravely restricts the effectiveness of RISs, and even incurs serious performance loss.

Recently, an upgraded version of RISs, termed simultaneously transmitting and reflecting RISs (STAR-RISs) has been proposed in [7]. In addition to inheriting the beneficial features of RISs, STAR-RISs have the following unique advantages: 1) Given their simultaneous control of transmitted and reflected signals, STAR-RISs are able to provide a full space smart radio environment; 2) By offering more degrees-of-freedoms (DoFs) for signal manipulation, STAR-RISs allow higher design flexibility [8]. Intuitively, a question is raised: *Can STAR-RISs achieve more reliable data transmission and higher energy efficiency for IoMT networks* than conventional reflecting-only RISs? To the best of our knowledge, there is a paucity of work that considered the application of RISs to IoMT networks, not to mention the integration of STAR-RISs.

Aroused by the above discussions, we investigate the trade-off between the secrecy and energy consumption in a STAR-RIS assisted IoMT network. The contributions of this paper are as follows: 1) We conceive the deployment of STAR-RIS in the IoMT network to secure telemedicine data transmission. From a practical point of view, the homebound patients (Bobs) are distributed on both sides of STAR-RIS in the presence of Eves, while all channel information is assumed to be imperfect. 2) We formulate a secrecy energy efficiency (SEE) maximization problem by designing the active and passive beamforming. The proposed robust design ensures that the achievable date rate at each Bob is no less than its minimum rate requirement for all possible channel error realizations. 3) Simulation results verify the SEE advantages of the proposed IoMT system over conventional RIS counterparts. The impacts of the maximum transmit power, the number of STAR-RIS elements and the CSI uncertainty (CSIU) on the SEE are shown numerically.

This work was supported by the National Key R&D Program of China under Grant No. 2020YFB1807801, and BUPT Innovation and Entrepreneurship Support Program under Grant No. 2022-YC-T010.

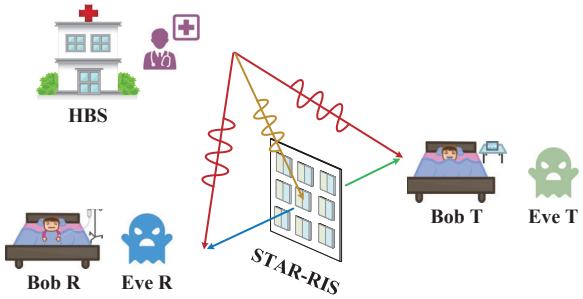

Fig. 1. System model of a STAR-RIS assisted secrecy IoMT network.

II. System Model and Problem Formulation

A. System Model

As shown in Fig. 1, we consider a STAR-RIS assisted IoMT network, where the hospital base station (HBS) sends telemedicine information to two homebound Bobs in the presence of two Eves. The transmission and reflection spaces are simultaneously served by STAR-RIS and both spaces have one Bob and one Eve. The sets of Bobs and Eves are denoted by $\mathcal{K}=\{U_r,U_t\}$ and $\mathcal{E}=\{E_r,E_t\}$, respectively. The STAR-RIS composes of M elements and the HBS is equipped with N antennas, while Bobs and Eves are all single-antenna.

Following the energy splitting (ES) protocol, each STAR-RIS element is simultaneously operated in the transmission mode ($\chi=t$) and the reflection mode ($\chi=r$) [7]. We denote $\mathbf{u}_\chi=\left[\sqrt{\beta_1^\chi}e^{j\theta_1^\chi},\sqrt{\beta_2^\chi}e^{j\theta_2^\chi},\ldots,\sqrt{\beta_M^\chi}e^{j\theta_M^\chi}\right]^{\mathrm{T}}\in\mathbb{C}^{M\times 1}$, $\forall m\in\mathcal{M}=\{1,2,\ldots,M\}$ as the transmission and reflection vectors, where $\left\{\sqrt{\beta_m^\chi}\in[0,1]\right\}$ and $\left\{\theta_m^\chi\in[0,2\pi)\right\}$ denote the amplitude and phase shifts coefficients of the m-th element operating in $\chi\in\{r,t\}$ modes, respectively. If Bob or Eve is located at the reflection space, we have $\mathbf{u}_\chi=\mathbf{u}_r$; otherwise $\mathbf{u}_\chi=\mathbf{u}_t$. The phase shifts of each element can be independently adjusted, while the amplitude coefficients are coupled due to the law of energy conservation, i.e., $\beta_m^t+\beta_m^r=1,\forall m$. The above constraints on STAR-RIS coefficients are given by

$$\mathbb{R}_{\beta,\theta}=\left\{\beta_m^\chi,\theta_m^\chi\middle|\sum\nolimits_\chi\beta_m^\chi=1;\beta_m^\chi\in[0,1];\theta_m^\chi\in[0,2\pi)\right\}. \quad (1)$$

Let $\mathbf{f}_k$ and s_k be the active beamforming vector and the desired signal for Bob k, $\forall k\in\mathcal{K}$, respectively, where $\mathbb{E}[|s_k|^2]=1$. Accordingly, the received signals at Bob k and Eve e, $\forall e\in\mathcal{E}$ are respectively given by

$$y_k=\bar{\mathbf{h}}_k\sum\nolimits_k\mathbf{f}_ks_k+n_k,\quad y_e=\bar{\mathbf{h}}_e\sum\nolimits_k\mathbf{f}_ks_k+n_e, \quad (2)$$

where $n_k\sim\mathcal{CN}(0,\sigma^2)$ and $n_e\sim\mathcal{CN}(0,\sigma^2)$ are the noises at Bob k and Eve e with zero mean and variance σ^2, respectively. Moreover, $\bar{\mathbf{h}}_k$ and $\bar{\mathbf{h}}_e$ are the combined channel gains from the HBS to Bob k and Eve e, respectively written as

$$\bar{\mathbf{h}}_k=\mathbf{h}_k^{\mathrm{H}}+\mathbf{u}_\chi^{\mathrm{H}}\mathbf{G}_k,\quad \bar{\mathbf{h}}_e=\mathbf{h}_e^{\mathrm{H}}+\mathbf{u}_\chi^{\mathrm{H}}\mathbf{G}_e, \quad (3)$$

where $\mathbf{G}_k=\mathrm{diag}(\mathbf{g}_k^{\mathrm{H}})\mathbf{H}_b\in\mathbb{C}^{M\times N}$, $\mathbf{G}_e=\mathrm{diag}(\mathbf{g}_e^{\mathrm{H}})\mathbf{H}_b\in\mathbb{C}^{M\times N}$ denote the cascaded links between the HBS and Bob k and between the HBS and Eve e, respectively. In addition, $\mathbf{h}_k^{\mathrm{H}}\in\mathbb{C}^{1\times N}$, $\mathbf{g}_k^{\mathrm{H}}\in\mathbb{C}^{1\times M}$, $\mathbf{H}_b\in\mathbb{C}^{M\times N}$, $\mathbf{h}_e^{\mathrm{H}}\in\mathbb{C}^{1\times N}$ and $\mathbf{g}_e^{\mathrm{H}}\in\mathbb{C}^{1\times M}$ are the channels from the HBS to Bob k, from the STAR-RIS to Bob k, from the HBS to STAR-RIS, from the HBS to Eve e, and from the STAR-RIS to Eve e, respectively.

We assume that all Bobs are the intended users of Eves. Then the achievable rate of Bob k and the eavesdropping rate of Eve e to decode s_k are respectively given by

$$R_k=\log_2\left(1+\frac{|\bar{\mathbf{h}}_k\mathbf{f}_k|^2}{|\bar{\mathbf{h}}_k\mathbf{f}_{\bar{k}}|^2+\sigma^2}\right),\ \forall k, \quad (4a)$$

$$R_k^e=\log_2\left(1+\frac{|\bar{\mathbf{h}}_e\mathbf{f}_k|^2}{|\bar{\mathbf{h}}_e\mathbf{f}_{\bar{k}}|^2+\sigma^2}\right),\ \forall k,e, \quad (4b)$$

where $\bar{k},k\in\mathcal{K},k\neq\bar{k}$. On this basis, the sum secrecy rate (SSR) of the system is given by $R_s=\sum_k\left[R_k-\sum_e R_k^e\right]^+$, where $[x]^+=\max\{x,0\}$. We omit $[\cdot]^+$ in the following due to the non-negative nature of the optimal secrecy rate.

In practice, various factors such as channel estimation and quantization errors would lead to outdated and coarse CSI. To this end, we adopt the bounded CSI model to characterize the uncertainties of CSI, given by [9]

$$\mathbf{h}_k=\hat{\mathbf{h}}_k+\triangle\mathbf{h}_k,\ \mathbf{G}_k=\hat{\mathbf{G}}_k+\triangle\mathbf{G}_k, \quad (5a)$$

$$\Omega_k=\{\|\triangle\mathbf{h}_k\|_2\leq\xi_k,\|\triangle\mathbf{G}_k\|_F\leq\zeta_k\}, \quad (5b)$$

$$\mathbf{h}_e=\hat{\mathbf{h}}_e+\triangle\mathbf{h}_e,\ \mathbf{G}_e=\hat{\mathbf{G}}_e+\triangle\mathbf{G}_e, \quad (5c)$$

$$\Omega_e=\{\|\triangle\mathbf{h}_e\|_2\leq\xi_e,\|\triangle\mathbf{G}_e\|_F\leq\zeta_e\}, \quad (5d)$$

where $\hat{\mathbf{h}}_k$ and $\hat{\mathbf{G}}_k$ are the estimations of $\mathbf{h}_k$ and $\mathbf{G}_k$, respectively. $\triangle\mathbf{h}_k$ and $\triangle\mathbf{G}_k$ are the channel estimation errors of $\mathbf{h}_k$ and $\mathbf{G}_k$, respectively. The continuous set Ω_k collects all possible channel estimation errors, with ξ_k and ζ_k denoting the radii of the uncertainty regions known at the HBS. $\hat{\mathbf{h}}_e$, $\hat{\mathbf{G}}_e$, $\triangle\mathbf{h}_e$ and $\triangle\mathbf{G}_e$ are defined similarly.

B. Problem Formulation

Our objective is to maximize the SEE while satisfying the secrecy and power constraints. Based on the secrecy capacity, the SEE is defined as the ratio of the SSR over the total power consumption [6]. Here, the total power dissipated to operate the considered system includes the HBS transmit power and the hardware static power P_0 can be modeled as [4]

$$\mathcal{P}=\varsigma\sum\nolimits_k\|\mathbf{f}_k\|_2^2+P_0, \quad (6)$$

where ς is a constant reflecting the power amplifier efficiency, $P_0=P_{\mathrm{B}}+2P_{\mathrm{U}}+MP_r(b)$, with P_{B}, P_{U} and $P_r(b)$ denoting the static power consumed by the HBS, each Bob and each phase shifter having b-bit resolution, respectively.

Armed with these definitions, by jointly designing the active beamforming $\mathbf{F}=\{\mathbf{f}_k|\forall k\}$ and the passive beamforming $\mathbf{U}=\{\mathbf{u}_\chi|\forall\chi\}$, the SEE maximization problem is formulated as

$$\max_{\mathbf{F},\mathbf{U}}\ \frac{\sum_k\left(R_k-\sum_e R_k^e\right)}{\varsigma\sum_k\|\mathbf{f}_k\|_2^2+P_0} \quad (7a)$$

$$\text{s.t.}\ \sum\nolimits_k\|\mathbf{f}_k\|_2^2\leq P_{\max}, \quad (7b)$$

$$\beta_m^\chi,\theta_m^\chi\in\mathbb{R}_{\beta,\theta},\ \forall\chi,m, \quad (7c)$$

$$R_k\geq C_k,\ \Omega_k,\forall k, \quad (7d)$$

$$R_k^e\leq C_k^e,\ \Omega_e,\ \forall k,e, \quad (7e)$$

where constraint (7b) represents that the total transmit power cannot exceed the budget $P_{\max}$, and constraint (7c) specifies the range of the reflection and transmission coefficients.

Moreover, constraint (7d) guarantees that the minimum rate requirement C_k is satisfied at Bob k, and C_k^e in (7e) denotes the maximum tolerable information leakage to Eve e for eavesdropping s_k. In particular, constraints (7d) and (7e) ensure that the SSR is bounded from below by $R_s \geq \sum_k \left[C_k - \sum_e C_k^e\right]^+$. Note that the operation $[\cdot]^+$ is omitted in the objective function (7a) since we can set $C_k \geq \sum_e C_k^e$ such that R_k is always greater or equal to $\sum_e R_k^e$.

We notice that problem (7) is hard to be solved directly due to the following reasons: 1) Compared to reflecting-only RISs, the newly introduced transmission and reflection coefficients are intricately coupled with the other variables; 2) Constraint (7c) is highly non-convex as each phase shifter is limited to the unit magnitude; 3) The CSI estimation error is considered in all involved channels, resulting in infinitely many non-convex constraints (7d) and (7e). To sum up, problem (7) is a non-convex problem, and is non-trivial to solve optimally.

III. Proposed Solutions

To solve problem (7) efficiently, we firstly reformulate it to an equivalent problem through introducing slack variables, which paves the way for decomposing the coupling variables. Next, relying on the $\mathcal{S}$-procedure and sign-definiteness, we transform the semi-definite constraints into the tractable forms. Then, the alternating optimization (AO) strategy is utilized to divide problem (25) into two subproblems.

To begin with, we introduce the slack variables ψ and ρ, and transform the original problem (7) into

$$\begin{aligned} \max_{\mathbf{F},\mathbf{U},\psi,\rho} \quad & \psi && \text{(8a)} \\ \text{s.t.} \quad & R_s \geq \psi\rho, && \text{(8b)} \\ & \mathcal{P} \leq t, && \text{(8c)} \\ & (7\text{b}) - (7\text{e}). && \text{(8d)} \end{aligned}$$

Obviously, constraint (8c) is a convex set, because it can be expressed as a second-order cone (SOC) representation:

$$\frac{\rho - P_0 + \varsigma}{2\varsigma} \geq \left\| \left[\frac{\rho - P_0 - \varsigma}{2\varsigma}, \mathbf{f}_t^{\mathrm{T}}, \mathbf{f}_r^{\mathrm{T}} \right]^{\mathrm{T}} \right\|_2. \tag{9}$$

In order to track the convexity of constraint (8b), we introduce the slack variable set $\mathbf{r} = \{r_k, r_k^e | \forall k, e\}$, satisfying $R_k = r_k$ and $R_k^e = r_k^e$. Furthermore, we employ the successive convex approximation (SCA) method to address the non-convex term $\psi\rho$. Specifically, using the first-order Taylor series (FTS), $\psi\rho$ can be upper bounded by $\psi\rho \leq (\psi\rho)^{\mathrm{ub}} = \psi\rho^{(\ell)} + \psi^{(\ell)}\rho - \psi^{(\ell)}\rho^{(\ell)}$, where $(\psi^{(\ell)}, \rho^{(\ell)})$ denotes the feasible point in the ℓ-th iteration. Then problem (8) is rewritten as

$$\begin{aligned} \max_{\mathbf{F},\mathbf{U},\psi,t,\mathbf{r}} \quad & \psi && \text{(10a)} \\ \text{s.t.} \quad & R_k \geq r_k, \ \Omega_k, \forall k, && \text{(10b)} \\ & R_k^e \leq r_k^e, \ \Omega_e, \forall k, e, && \text{(10c)} \\ & r_k \geq C_k, \ \forall k, && \text{(10d)} \\ & r_k^e \leq C_k^e, \ \forall k, e, && \text{(10e)} \\ & \sum\nolimits_k (r_k - \sum\nolimits_e r_k^e) \geq (\psi\rho)^{\mathrm{ub}}, \ \forall k, e, && \text{(10f)} \\ & (7\text{b}), (7\text{c}), (9). && \text{(10g)} \end{aligned}$$

Now the main difficulty in problem (10) is the semi-definite constraints (10b) and (10c). To this end, we construct finite linear matrix inequalities (LMIs) equivalent to them as follows.

A. Semi-Infinite Constraint Transformation

With the aid of the slack variable set $\boldsymbol{\eta} = \{\eta_k, \eta_k^e | \forall k, e\}$, constraints (10b) and (10c) are respectively rewritten as

$$\begin{aligned} & |\bar{\mathbf{h}}_k \mathbf{f}_k|^2 \geq \eta_k (2^{r_k} - 1), \ \Omega_k, \forall k, && \text{(11a)} \\ & |\bar{\mathbf{h}}_k \mathbf{f}_{\bar{k}}|^2 \ + \ \sigma^2 \leq \eta_k, \ \Omega_k, \forall k, && \text{(11b)} \\ & |\bar{\mathbf{h}}_e \mathbf{f}_k|^2 \leq \eta_k^e (2^{r_k^e} - 1), \ \Omega_e, \forall k, e, && \text{(11c)} \\ & |\bar{\mathbf{h}}_e \mathbf{f}_{\bar{k}}|^2 \ + \ \sigma^2 \geq \eta_k^e, \ \Omega_e, \forall k, e. && \text{(11d)} \end{aligned}$$

Given the uncertainty of CSI, the constraints in (11) all have infinite possibilities. To tackle constraint (11a), we first derive its linear approximation in the following proposition.

***Proposition** 1: Denoting $(\mathbf{F}^{(\ell)}, \mathbf{U}^{(\ell)})$ as the optimal solutions obtained in the ℓ-th iteration, constraint (11a) can be equivalently linearized by*

$$\mathbf{x}_k^{\mathrm{H}} \mathbf{A}_k \mathbf{x}_k + 2\mathrm{Re}\{\mathbf{a}_k^{\mathrm{H}} \mathbf{x}_k\} + a_k \geq \eta_k (2^{r_k} - 1), \ \Omega_k, \forall k, \tag{12}$$

where the introduced coefficients $\mathbf{x}_k$, $\mathbf{A}_k$, $\mathbf{a}_k$ and a_k are given as (13) at the bottom of the next page.

Proof: Based on the FTS, a lower bound of the convex term $|\bar{\mathbf{h}}_k \mathbf{f}_k|^2$ can be expressed as the right-hand of (14) at the bottom of the next page. Moreover, by substituting (5a) into (14) and performing further mathematical transformations, we can obtain (12) and the proof is completed. □

Although constraint (11a) is transformed into more tractable linear form in (12), there are still an infinite number of such LMIs in (12). To facilitate derivation, we resort to the $\mathcal{S}$-procedure to further convert them into a manageable form.

***Lemma** 1: ($\mathcal{S}$-procedure [10]) Let a quadratic function $f_j(\mathbf{x})$, $\mathbf{x} \in \mathbb{C}^{N\times 1}$, $j \in \mathcal{J} = \{0, 1, \ldots, J\}$, be defined as*

$$f_j(\mathbf{x}) = \mathbf{x}^{\mathrm{H}} \mathbf{A}_j \mathbf{x} + 2\mathrm{Re}\{\mathbf{a}_j^{\mathrm{H}} \mathbf{x}\} + a_j, \tag{15}$$

where $\mathbf{A}_j \in \mathbb{H}^N$, $\mathbf{a}_j \in \mathbb{C}^{N\times 1}$, and $a_j \in \mathbb{R}$. Then the condition $\{f_j(\mathbf{x}) \geq 0\}_{j=1}^J \Rightarrow f_0(\mathbf{x}) \geq 0$ holds if and only if there exist $\upsilon_j \geq 0, \forall j \in \mathcal{J}$ such that

$$\begin{bmatrix} \mathbf{A}_0 & \mathbf{a}_0 \\ \mathbf{a}_0^{\mathrm{H}} & a_0 \end{bmatrix} - \sum\nolimits_{j=1}^J \upsilon_j \begin{bmatrix} \mathbf{A}_j & \mathbf{a}_j \\ \mathbf{a}_j^{\mathrm{H}} & a_j \end{bmatrix} \succeq \mathbf{0}. \tag{16}$$

Since $\|\triangle \mathbf{h}_k\|_2 \leq \xi_k$ is equivalent to $\triangle \mathbf{h}_k^{\mathrm{H}} \triangle \mathbf{h}_k \leq \xi_k^2$, we can express Ω_k in terms of the quadratic expression as

$$\Omega_k \triangleq \begin{cases} \mathbf{x}_k^{\mathrm{H}} \mathbf{C}_1 \mathbf{x}_k - \xi_k^2 \leq 0, \\ \mathbf{x}_k^{\mathrm{H}} \mathbf{C}_2 \mathbf{x}_k - \zeta_k^2 \leq 0. \end{cases} \forall k, \tag{17}$$

where $\mathbf{C}_1 = \begin{bmatrix} \mathbf{I}_N & \mathbf{0} \\ \mathbf{0} & \mathbf{0} \end{bmatrix}$ and $\mathbf{C}_2 = \begin{bmatrix} \mathbf{0} & \mathbf{0} \\ \mathbf{0} & \mathbf{I}_{MN} \end{bmatrix}$. Then according to Lemma 1, the implication (17)⇒(12) holds if and only if there exist $\upsilon_k^h \geq 0$ and $\upsilon_k^G \geq 0$ such that

$$\begin{bmatrix} \mathbf{A}_k + \upsilon_k^h \mathbf{C}_1 + \upsilon_k^G \mathbf{C}_2 & \mathbf{a}_k \\ \mathbf{a}_k^{\mathrm{H}} & Q_k \end{bmatrix} \succeq \mathbf{0}, \ \forall k, \tag{18}$$

where $Q_k = a_k - \eta_k(2^{r_k} - 1) - \upsilon_k^h \xi_k^2 - \upsilon_k^G \zeta_k^2$.

Using the same method, constraint (11d) is rewritten as

$$\begin{bmatrix} \mathbf{A}_k^e + \upsilon_k^{e,h} \mathbf{C}_1 + \upsilon_k^{e,G} \mathbf{C}_2 & \mathbf{a}_k^e \\ (\mathbf{a}_k^e)^{\mathrm{H}} & Q_k^e \end{bmatrix} \succeq \mathbf{0}, \ \forall k, e, \tag{19}$$

where $\upsilon_k^{e,h}, \upsilon_k^{e,G} \geq 0$, $Q_k^e = a_k^e - \eta_k^e + \sigma^2 - \upsilon_k^{e,h}\xi_e^2 - \upsilon_k^{e,G}\zeta_e^2$. $\mathbf{A}_{\bar{k}}^e$, $\mathbf{a}_{\bar{k}}^e$ and $a_{\bar{k}}^e$ are obtained by replacing $\mathbf{f}_k$ with $\mathbf{f}_{\bar{k}}$, $\mathbf{f}_{\bar{k}}^{(\ell)}$ with $\mathbf{f}_{\bar{k}}^{(\ell)}$, $\hat{\mathbf{h}}_k$ with $\hat{\mathbf{h}}_e$, and $\hat{\mathbf{G}}_k$ with $\hat{\mathbf{G}}_e$ in $\mathbf{A}_k$, $\mathbf{a}_k$ and a_k, respectively.

About constraint (11b), by applying the Schur's complement Lemma [11], considering the uncertainty in $\mathbf{h}_k$ and $\mathbf{G}_k$, and denoting $\pi_k = ((\hat{\mathbf{h}}_k^{\mathrm{H}} + \mathbf{u}_\chi^{\mathrm{H}}\hat{\mathbf{G}}_k)\mathbf{f}_{\bar{k}})^*$, (11b) can be recast as (20) at the bottom of this page. To deal with the multiple complex valued uncertainties involved in (20b), we formally introduce the general sign-definiteness lemma as follows.

***Lemma** 2: (General sign-definiteness [12]) Given matrices $\mathbf{A}$ and $\{\mathbf{E}_j, \mathbf{F}_j\}_{j=1}^J$ with $\mathbf{A} = \mathbf{A}^{\mathrm{H}}$, the semi-infinite LMI*

$$\mathbf{A} \succeq \sum\nolimits_{j=1}^{J} \left(\mathbf{E}_j^{\mathrm{H}}\mathbf{G}_j\mathbf{F}_j + \mathbf{F}_j^{\mathrm{H}}\mathbf{G}_j^{\mathrm{H}}\mathbf{E}_j\right),\ \forall j, \|\mathbf{G}_j\|_F \leq \xi_j, \quad (21)$$

holds if and only if there exist $\varpi_j \geq 0, \forall j$, such that

$$\begin{bmatrix} \mathbf{A} - \sum_{j=1}^{J} \varpi_j \mathbf{F}_j^{\mathrm{H}}\mathbf{F}_j & -\xi_1\mathbf{E}_1^{\mathrm{H}} & \cdots & -\xi_J\mathbf{E}_J^{\mathrm{H}} \\ -\xi_1\mathbf{E}_1 & \varpi_1\mathbf{I} & \cdots & \mathbf{0} \\ \vdots & \vdots & \ddots & \vdots \\ -\xi_J\mathbf{E}_J & \mathbf{0} & \cdots & \varpi_J\mathbf{I} \end{bmatrix} \succeq \mathbf{0}. \quad (22)$$

Afterwards, by applying Lemma 2, the equivalent LMIs of constraint (20b) can be expressed as

$$\begin{bmatrix} T_k & \pi_k^* & \mathbf{0}_{1\times N} & \mathbf{0}_{1\times N} \\ \pi_k & 1 & \xi_k\mathbf{f}_{\bar{k}}^{\mathrm{H}} & \zeta_k\mathbf{f}_{\bar{k}}^{\mathrm{H}} \\ \mathbf{0}_{N\times 1} & \xi_k\mathbf{f}_{\bar{k}} & \varpi_k^h\mathbf{I}_N & \mathbf{0}_N \\ \mathbf{0}_{N\times 1} & \zeta_k\mathbf{f}_{\bar{k}} & \mathbf{0}_N & \varpi_k^G\mathbf{I}_N \end{bmatrix} \succeq \mathbf{0},\ \forall k, \quad (23)$$

where ϖ_k^h, $\varpi_k^G \geq 0$ are the introduced slack variables, and $T_k = \eta_k - \sigma^2 - \varpi_k^h\sum_m \beta_m^\chi - \varpi_k^G$. Similarly, with $\varpi_k^{e,h}$, $\varpi_k^{e,G} \geq 0$, it is possible to rewrite (11c) as the following finite LMIs

$$\begin{bmatrix} T_k^e & (\pi_k^e)^* & \mathbf{0}_{1\times N} & \mathbf{0}_{1\times N} \\ \pi_k^e & 1 & \xi_e\mathbf{f}_k^{\mathrm{H}} & \zeta_e\mathbf{f}_k^{\mathrm{H}} \\ \mathbf{0}_{N\times 1} & \xi_e\mathbf{f}_k & \varpi_k^{e,h}\mathbf{I}_N & \mathbf{0}_N \\ \mathbf{0}_{N\times 1} & \zeta_e\mathbf{f}_k & \mathbf{0}_N & \varpi_k^{e,G}\mathbf{I}_N \end{bmatrix} \succeq \mathbf{0},\ \forall k, e, \quad (24)$$

where $T_k^e = \eta_k^e(2^{r_k^e} - 1) - \varpi_k^{e,h}\sum_m \beta_m^\chi - \varpi_k^{e,G}$ and $\pi_k^e = ((\hat{\mathbf{h}}_e^{\mathrm{H}} + \mathbf{u}_\chi^{\mathrm{H}}\hat{\mathbf{G}}_e)\mathbf{f}_k)^*$. Eventually, reformulating problem (10) by replacing constraints (10b) and (10c) with the LMIs (18), (19), (23) and (24) yields the following problem

$$\max_{\mathbf{F},\mathbf{U},\boldsymbol{\Delta}} \quad \psi \quad (25a)$$

$$\text{s.t.} \quad (7\text{b}), (7\text{c}), (9), (10\text{d}) - (10\text{f}), \quad (25b)$$

$$(18), (19), (23), (24), \quad (25c)$$

$$\upsilon_k^h, \upsilon_k^G, \upsilon_k^{e,h}, \upsilon_k^{e,G} \geq 0,\ \forall k, e, \quad (25d)$$

$$\varpi_k^h, \varpi_k^G, \varpi_k^{e,h}, \varpi_k^{e,G} \geq 0,\ \forall k, e, \quad (25e)$$

where $\boldsymbol{\Delta} = \{\psi, \rho, \mathbf{r}, \boldsymbol{\eta}, \boldsymbol{\upsilon}, \boldsymbol{\varpi}\}$ denotes the set of all auxiliary variables, with $\boldsymbol{\upsilon} = \{\upsilon_k^h, \upsilon_k^G, \upsilon_k^{e,h}, \upsilon_k^{e,G} | \forall k, e\}$ and $\boldsymbol{\varpi} = \{\varpi_k^h, \varpi_k^G, \varpi_k^{e,h}, \varpi_k^{e,G} | \forall k, e\}$.

Note that problem (25) is still non-convex and challenging to optimize $\mathbf{F}$ and $\mathbf{U}$ simultaneously, since they are highly coupled in parameters such as $\mathbf{A}_k$, $\mathbf{a}_k$ and π_k. To solve it, we employ the AO strategy to decouple the optimization variables and transform problem (25) into two subproblems.

B. Active Beamforming Design

For given $\mathbf{U}$, the optimization problem for the design of the active beamforming $\mathbf{F}$ can be formulated as

$$\max_{\mathbf{F},\boldsymbol{\Delta}} \quad \psi \quad (26a)$$

$$\text{s.t.} \quad (7\text{b}), (9), (10\text{d}) - (10\text{f}), \quad (26b)$$

$$(18), (19), (23), (24), (25\text{d}), (25\text{e}). \quad (26c)$$

At this point, it is noticed that all the constraints in problem (26) are convex except (18). Moreover, its non-convexity arises from the term $\eta_k 2^{r_k}$ in Q_k. To proceed, we leverage the SCA approach to obtaining approximation. Specifically, for a given feasible point $(\eta_k^{(\ell)}, r_k^{(\ell)})$ in the ℓ-th iteration, $\eta_k 2^{r_k}$ is upper bounded by $\left((r_k - r_k^{(\ell)})\eta_k^{(\ell)}\ln 2 + \eta_k\right)2^{r_k^{(\ell)}}$. As a result, we can recast problem (26) as

$$\max_{\mathbf{F},\boldsymbol{\Delta}} \quad \psi \quad (27a)$$

$$\text{s.t.} \quad (26\text{b}), (19), (23), (24), (25\text{d}), (25\text{e}), \quad (27b)$$

$$\begin{bmatrix} \mathbf{A}_k + \upsilon_k^h\mathbf{C}_1 + \upsilon_k^G\mathbf{C}_2 & \mathbf{a}_k \\ \mathbf{a}_k^{\mathrm{H}} & \widehat{Q}_k \end{bmatrix} \succeq \mathbf{0},\ \forall k, \quad (27c)$$

$$\mathbf{x}_k = \left[\triangle\mathbf{h}_k^{\mathrm{H}}\ \mathrm{vec}^{\mathrm{H}}(\triangle\mathbf{G}_k^*)\right]^{\mathrm{H}},\ \mathbf{A}_k = \widetilde{\mathbf{A}}_k + \widetilde{\mathbf{A}}_k^{\mathrm{H}} - \widehat{\mathbf{A}}_k,\ \mathbf{a}_k = \widetilde{\mathbf{a}}_k + \widehat{\mathbf{a}}_k - \bar{\mathbf{a}}_k,\ a_k = 2\mathrm{Re}\{\widetilde{a}_k\} - \widehat{a}_k, \quad (13a)$$

$$\widetilde{\mathbf{A}}_k = \begin{bmatrix} \mathbf{f}_k^{(\ell)} \\ \mathbf{f}_k^{(\ell)} \otimes (\mathbf{u}_\chi^{(\ell)})^* \end{bmatrix}\left[\mathbf{f}_k^{\mathrm{H}}\ \mathbf{f}_k^{\mathrm{H}} \otimes \mathbf{u}_\chi^{\mathrm{T}}\right],\ \widehat{\mathbf{A}}_k = \begin{bmatrix} \mathbf{f}_k^{(\ell)} \\ \mathbf{f}_k^{(\ell)} \otimes (\mathbf{u}_\chi^{(\ell)})^* \end{bmatrix}\left[(\mathbf{f}_k^{(\ell)})^{\mathrm{H}}\ (\mathbf{f}_k^{(\ell)})^{\mathrm{H}} \otimes (\mathbf{u}_\chi^{(\ell)})^{\mathrm{T}}\right], \quad (13b)$$

$$\widetilde{\mathbf{a}}_k = \begin{bmatrix} \mathbf{f}_k(\mathbf{f}_k^{(\ell)})^{\mathrm{H}}(\hat{\mathbf{h}}_k + \hat{\mathbf{G}}_k^{\mathrm{H}}\mathbf{u}_\chi^{(\ell)}) \\ \mathrm{vec}^*(\mathbf{u}_\chi(\hat{\mathbf{h}}_k^{\mathrm{H}} + (\mathbf{u}_\chi^{(\ell)})^{\mathrm{H}}\hat{\mathbf{G}}_k)\mathbf{f}_k^{(\ell)}\mathbf{f}_k^{\mathrm{H}}) \end{bmatrix},\ \widehat{\mathbf{a}}_k = \begin{bmatrix} \mathbf{f}_k^{(\ell)}\mathbf{f}_k^{\mathrm{H}}(\hat{\mathbf{h}}_k + \hat{\mathbf{G}}_k^{\mathrm{H}}\mathbf{u}_\chi) \\ \mathrm{vec}^*(\mathbf{u}_\chi^{(\ell)}(\hat{\mathbf{h}}_k^{\mathrm{H}} + \mathbf{u}_\chi^{\mathrm{H}}\hat{\mathbf{G}}_k)\mathbf{f}_k(\mathbf{f}_k^{(\ell)})^{\mathrm{H}}), \end{bmatrix}, \quad (13c)$$

$$\bar{\mathbf{a}}_k = \begin{bmatrix} \mathbf{f}_k^{(\ell)}(\mathbf{f}_k^{(\ell)})^{\mathrm{H}}(\hat{\mathbf{h}}_k + \hat{\mathbf{G}}_k^{\mathrm{H}}\mathbf{u}_\chi^{(\ell)}) \\ \mathrm{vec}^*(\mathbf{u}_\chi^{(\ell)}(\hat{\mathbf{h}}_k^{\mathrm{H}} + (\mathbf{u}_\chi^{(\ell)})^{\mathrm{H}}\hat{\mathbf{G}}_k)\mathbf{f}_k^{(\ell)}(\mathbf{f}_k^{(\ell)})^{\mathrm{H}}), \end{bmatrix}, \quad (13d)$$

$$\widetilde{a}_k = (\hat{\mathbf{h}}_k^{\mathrm{H}} + (\mathbf{u}_\chi^{(\ell)})^{\mathrm{H}}\hat{\mathbf{G}}_k)\mathbf{f}_k^{(\ell)}\mathbf{f}_k^{\mathrm{H}}(\hat{\mathbf{h}}_k + \hat{\mathbf{G}}_k^{\mathrm{H}}\mathbf{u}_\chi),\ \widehat{a}_k = (\hat{\mathbf{h}}_k^{\mathrm{H}} + (\mathbf{u}_\chi^{(\ell)})^{\mathrm{H}}\hat{\mathbf{G}}_k)\mathbf{f}_k^{(\ell)}(\mathbf{f}_k^{(\ell)})^{\mathrm{H}}(\hat{\mathbf{h}}_k + \hat{\mathbf{G}}_k^{\mathrm{H}}\mathbf{u}_\chi^{(\ell)}). \quad (13e)$$

$$|\bar{\mathbf{h}}_k\mathbf{f}_k|^2 \geq 2\mathrm{Re}\left\{(\mathbf{h}_k^{\mathrm{H}} + (\mathbf{u}_\chi^{(\ell)})^{\mathrm{H}}\mathbf{G}_k)\mathbf{f}_k^{(\ell)}\mathbf{f}_k^{\mathrm{H}}(\mathbf{h}_k + \mathbf{G}_k^{\mathrm{H}}\mathbf{u}_\chi)\right\} - (\mathbf{h}_k^{\mathrm{H}} + (\mathbf{u}_\chi^{(\ell)})^{\mathrm{H}}\mathbf{G}_k)\mathbf{f}_k^{(\ell)}(\mathbf{f}_k^{(\ell)})^{\mathrm{H}}(\mathbf{h}_k + \mathbf{G}_k^{\mathrm{H}}\mathbf{u}_\chi^{(\ell)}). \quad (14)$$

$$\mathbf{0} \preceq \begin{bmatrix} \eta_k - \sigma^2 & \pi_k^* \\ \pi_k & 1 \end{bmatrix} + \begin{bmatrix} 0 & \left(\triangle\mathbf{h}_k^{\mathrm{H}} + \mathbf{u}_\chi^{\mathrm{H}}\triangle\mathbf{G}_k\right)\mathbf{f}_{\bar{k}} \\ \mathbf{f}_{\bar{k}}^{\mathrm{H}}\left(\triangle\mathbf{h}_k + \triangle\mathbf{G}_k^{\mathrm{H}}\mathbf{u}_\chi\right) & 0 \end{bmatrix} \quad (20a)$$

$$\preceq \begin{bmatrix} \mathbf{0} \\ \mathbf{f}_{\bar{k}}^{\mathrm{H}} \end{bmatrix}\begin{bmatrix} \triangle\mathbf{h}_k & \mathbf{0} \end{bmatrix} + \begin{bmatrix} \triangle\mathbf{h}_k^{\mathrm{H}} \\ \mathbf{0} \end{bmatrix}\begin{bmatrix} \mathbf{0} & \mathbf{f}_{\bar{k}} \end{bmatrix} + \begin{bmatrix} \mathbf{0} \\ \mathbf{f}_{\bar{k}}^{\mathrm{H}} \end{bmatrix}\triangle\mathbf{G}_k^{\mathrm{H}}\begin{bmatrix} \mathbf{u}_\chi & \mathbf{0} \end{bmatrix} + \begin{bmatrix} \mathbf{u}_\chi^{\mathrm{H}} \\ \mathbf{0} \end{bmatrix}\triangle\mathbf{G}_k\begin{bmatrix} \mathbf{0} & \mathbf{f}_{\bar{k}} \end{bmatrix} + \begin{bmatrix} \eta_k - \sigma^2 & \pi_k^* \\ \pi_k & 1 \end{bmatrix}. \quad (20b)$$

where $\widehat{Q}_k = a_k + \eta_k - \big((r_k - r_k^{(\ell)})\eta_k^{(\ell)}\ln 2 + \eta_k\big)2^{r_k^{(\ell)}} - \upsilon_k^h\xi_k^2 - \upsilon_k^G\zeta_k^2$. Obviously, problem (27) is a convex semidefinite program (SDP), which can be solved efficiently via the CVX.

C. Passive Beamforming Design

With fixed $\mathbf{F}$, we arrive at the optimization of the transmission and reflection beamforming $\mathbf{U}$. As the non-convex constraint (18) is also an obstacle to this subproblem, we utilize the procedure devised above to address it. Armed with (27c), the subproblem for $\mathbf{U}$ is given by

$$\max_{\mathbf{U},\boldsymbol{\Delta}} \quad \psi \tag{28a}$$
$$\text{s.t.} \quad (9), (10\text{d}) - (10\text{f}), (27\text{c}), \tag{28b}$$
$$(19), (23), (24), (25\text{d}), (25\text{e}), \tag{28c}$$
$$\sum\nolimits_{\chi} \beta_m^{\chi} = 1,\ \beta_m^{\chi} \in [0,1],\ \forall \chi, m, \tag{28d}$$
$$[\mathbf{u}_\chi]_m = \sqrt{\beta_m^{\chi}} e^{j\theta_m^{\chi}},\ \theta_m^{\chi} \in [0, 2\pi),\ \forall \chi, m. \tag{28e}$$

Note that the remaining difficulty for solving problem (28) is the unit-modulus constraint (28e), which can be handled by the penalty convex-concave procedure (CCP) method.

In particular, the auxiliary variable set $\mathbf{b} = \{b_{\chi,m} | \forall \chi, m\}$ is introduced to linearize constraint (28e), which satisfies $b_{\chi,m} = [\mathbf{u}_\chi]_m^*[\mathbf{u}_\chi]_m$. Then we can rewrite $b_{\chi,m} = [\mathbf{u}_\chi]_m^*[\mathbf{u}_\chi]_m$ as $b_{\chi,m} \le [\mathbf{u}_\chi]_m^*[\mathbf{u}_\chi]_m \le b_{\chi,m}$. Based on the FTS, the non-convex part $b_{\chi,m} \le [\mathbf{u}_\chi]_m^*[\mathbf{u}_\chi]_m$ can be approximated by $b_{\chi,m} \le 2\text{Re}\big\{[\mathbf{u}_\chi]_m^*[\mathbf{u}_\chi^{(\ell)}]_m\big\} - [\mathbf{u}_\chi^{(\ell)}]_m^*[\mathbf{u}_\chi^{(\ell)}]_m$. On this basis, we penalize these terms which are included in the objective function (28a), and reformulate problem (28) as

$$\max_{\mathbf{U},\boldsymbol{\Delta},\mathbf{b},\mathbf{c}} \quad \psi - \lambda^{(\ell)} C \tag{29a}$$
$$\text{s.t.} \quad (28\text{b}), (28\text{c}), \tag{29b}$$
$$[\mathbf{u}_\chi]_m^*[\mathbf{u}_\chi]_m \le b_{\chi,m} + c_{\chi,m},\ \forall \chi, m, \tag{29c}$$
$$2\text{Re}\big\{[\mathbf{u}_\chi]_m^*[\mathbf{u}_\chi^{(\ell)}]_m\big\} - [\mathbf{u}_\chi^{(\ell)}]_m^*[\mathbf{u}_\chi^{(\ell)}]_m \ge b_{\chi,m} - \hat{c}_{\chi,m},\ \forall \chi, m, \tag{29d}$$
$$\sum\nolimits_{\chi} b_{\chi,m} = 1,\ b_{\chi,m} \ge 0,\ \forall \chi, m, \tag{29e}$$

where $\mathbf{c} = \{c_{\chi,m}, \hat{c}_{\chi,m} | \forall \chi, m\}$ is the slack variable set imposed over modulus constraints. $C = \sum_\chi \sum_m (c_{\chi,m} + \hat{c}_{\chi,m})$ is the penalty term, and is scaled by the regularization factor $\lambda^{(\ell)}$, which controls the feasibility of the constraints. $\lambda^{(\ell)}$ can be updated in the ℓ-th iteration by $\lambda^{(\ell)} = \min\{\varepsilon\lambda^{(\ell-1)}, \lambda_{\max}\}$, where $\varepsilon > 1$ and $\lambda_{\max}$ is the maximum value introduced to avoid a numerical problem. Problem (29) is a convex SDP and can be effectively solved by the existing toolbox.

D. Complexity and Convergence Analysis

Following the AO framework, problem (7) can be solved by solving problems (27) and (29) in an iterative manner. It can be observed that these resulting convex problems contain the LMI, SOC constraints and linear constraints, thus all problems can be solved by the interior point method [11]. Specifically, by ignoring the non-dominated linear constraints, the general expression for complexity is provided in [9]. Then the complexity of solving problems (27) and (29) is given by $\mathcal{O}_{\mathbf{F}} = \mathcal{O}(M^{3.5}N^{4.5})$ and $\mathcal{O}_{\mathbf{U}} = \mathcal{O}(M^{4.5}N^{3.5})$, respectively. Furthermore, let I_{iter} denote the number of iterations needed for the convergence of the proposed AO algorithm, the overall complexity is given by $\mathcal{O}(I_{iter}(\mathcal{O}_{\mathbf{F}} + \mathcal{O}_{\mathbf{U}}))$. On the other hand, since each sub-algorithm converges to their individual sub-optimal solution [9], the objective value of problem (7) is non-decreasing in each AO iteration, and is upper bounded by a finite value. Hence, the proposed AO algorithm can be guaranteed to converge.

IV. Simulation Results

In this section, numerical results are provided to verify the performance of the proposed robust design. We assume that the HBS and the STAR-RIS are located at $(0, 0, 10)$ and $(0, 30, 20)$ m, respectively. Bobs and Eves are randomly distributed in their own circle with the radius of 4 m. Moreover, Bob and Eve in reflection space are centered on $(0, 25, 0)$ and $(15, 25, 0)$ m, while the corresponding centers in transmission space are $(0, 35, 0)$ and $(15, 35, 0)$ m, respectively. We adopt Rician fading for all channels. To facilitate the presentation, we define κ_k^h, κ_k^G, κ_e^h and κ_e^G as the maximum normalized estimation errors for $\mathbf{h}_k$, $\mathbf{G}_k$, $\mathbf{h}_e$ and $\mathbf{G}_e$, e.g., $\kappa_k^h = \frac{\xi_k}{\|\hat{\mathbf{h}}_k\|_2}$. Besides, we set $\sigma^2 = -80$ dBm, $\varsigma = 1$, $P_{\text{B}} = 10$ dBW, $P_{\text{U}} = 10$ dBm [4], $C_k = 1.5$ bits/s/Hz, and $C_k^e = 0.6$ bits/s/Hz, $\forall k, e$.

Here, we compare the proposed design with three baselines: 1) Uniform ES (UES), where all ES elements employ the same transmission and reflection amplitude coefficients, i.e., $\beta_m^{\chi} = \beta^{\chi}$, $\beta^{\chi} \in [0, 1]$, $\sum_\chi \beta^{\chi} = 1$, $\forall \chi, m$ [7]; 2) Equal time splitting (ETS), where the STAR-RIS switches all elements between two modes in equal orthogonal periods, and the HBS sends signal to two spaces in different time periods; 3) RIS, where a reflecting-only RIS and a transmitting-only RIS are deployed adjacent to each other, and each has $M/2$ elements.

Fig. 2 depicts the achievable SEE versus the maximum transmit power $P_{\max}$. It is intuitive that the SEE of all the schemes increase first with $P_{\max}$ and eventually saturate. The reason is that the SEE maximization reduces to the SSR maximization for low $P_{\max}$, and using full power is optimal. While the power availability is sufficient, further increase of the SSR generates repaid elevation of energy consumption. Thus, the optimal strategy for large $P_{\max}$ is maintaining the power equal to the finite maximizer of the SEE. Another observation is that ETS is preferable for low $P_{\max}$, while ES achieves the best for high $P_{\max}$. The reason behind this is twofold. On the one hand, the interference-free transmission implemented by ETS facilitates the legitimate rate improvement at limited power. However, for larger $P_{\max}$, the inter-cluster interference brought by ES can be used to deteriorate the reception of Eves, thereby enhancing the SEE. On the other hand, since ETS only serves one side in each instant, there is always an Eve not suppressed by STAR-RIS. As a result, ETS suffers from more severe performance loss than ES, UES or even RIS.

Regarding the performance comparison between ES and UES, ES and RIS, as illustrated in Fig. 2, ES performs better than the two. This is because compared with ES which employs independent amplitude and phase shift models, UES and RIS have limited control of reflection and transmission

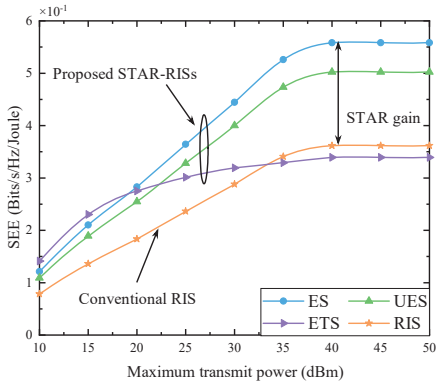

Fig. 2. SEE versus $P_{\max}$ for $M=20$, $N=4$, $\kappa_k^h=\kappa_k^G=\kappa_e^h=\kappa_e^G=0.2$ and $P_r(b)=10$ mW.

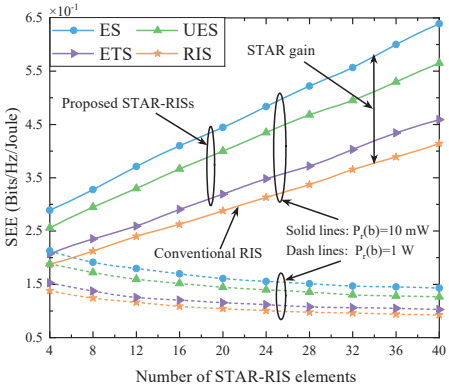

Fig. 3. SEE versus M for $P_{\max}=30$ dBm, $N=4$, and $\kappa_k^h=\kappa_k^G=\kappa_e^h=\kappa_e^G=0.2$.

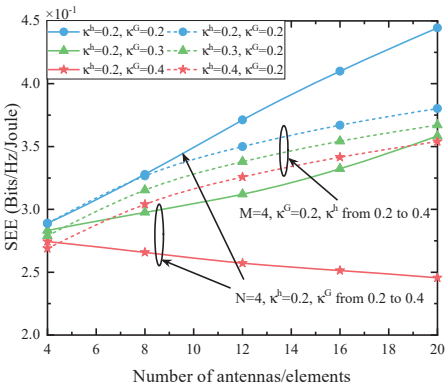

Fig. 4. SEE versus N, M and CSIU levels, for $P_{\max}=30$ dBm and $P_r(b)=10$ mW.

coefficients. Specifically, UES employs the group-wise amplitude control, while RIS employs fixed element-based mode selection. In comparison, by adjusting phase shift coefficients in an element-wise manner, ES can fully exploit the DoFs available at each element to enhance the desired signal, mitigate inter-user interference and inhibit bilateral eavesdropping. Additionally, this phenomenon can also be explained by the fact that both UES and RIS are special cases of ES.

Fig. 3 characterizes the SEE versus the number of elements M for different bit resolution power consumption $P_r(b)$. As clearly shown, when $P_r(b)=10$ mW, all designs exhibit the same trend that the SEE performance continues to increase with M. This indicates that this value of $P_r(b)$ is quite small, and the increase of M will not cause significant energy consumption cost. Indeed, the extra spatial DoFs offered by the large-scale STAR-RIS can provide a stronger cascaded channel for Bobs but substantially suppress information leakage. Unfortunately, for higher values of $P_r(b)$, the STAR-RIS power consumption becomes one of the dominant items of energy efficiency. As such, the SEE starts decreasing even for a small-to-moderate M value. In other words, there exists a trade-off between the secure performance benefit of deploying the large scale STAR-RIS and its power consumption. Furthermore, it is evident that the ES STAR-RIS assisted system achieves larger SEE than RISs counterparts, which again demonstrates the superiority of the proposed system design.

Fig. 4 illustrates the obtained SEE under ES versus the number of the transmit antennas N and the number of elements M under different CSIUs. We set $\kappa^h=\kappa_k^h=\kappa_e^h$ and $\kappa^G=\kappa_k^G=\kappa_e^G$. In Fig. 4, for the cases with fixed N, the SEE under low CSIU, e.g., $\kappa^h=0.2$, $\kappa^G=\{0.2,0.3\}$, increases with an increment of M. This is in agreement with Fig. 3. However, when $\kappa^G=0.4$, the SEE starts to decrease with the increase of M. This reveals that, a serious channel estimation error will be introduced with a larger M under high-level CSIU, which hinders the improvement of SEE as M grows. By contrast, when fixing M, the SEE still raises steadily as N grows even at higher CSIU. The reason is that, more DoFs to the active beamforming are offered by the increase of N, which is enough to compensate for the channel estimation error.

V. Conclusion

This paper studied the secure and efficient telemedicine communication in the STAR-RIS aided IoMT networks. Considering the imperfect CSI, we formulated a non-convex SEE maximization problem by jointly designing the active and passive beamforming. A robust resource allocation algorithm was developed by invoking AO, SCA and penalty CCP methods. Numerical results verified the superiority of STAR-RISs and provided helpful insights for the practical system design.

References

[1] A. Ghubaish, T. Salman, and M. Zolanvari *et al*, "Recent advances in the Internet-of-Medical-Things (IoMT) systems security," *IEEE Internet Things J.*, vol. 8, no. 11, pp. 8707-8718, Jun, 2021.

[2] S. Maji *et al.*, "A low-power dual-factor authentication unit for secure implantable devices," in *Proc. IEEE Custom Integr. Circuits Conf. (CICC)*, Boston, MA, USA, 2020, pp. 1–4.

[3] M. Kumar and S. A. Chand, "A secure and efficient cloud-centric Internet-of-Medical-Things-enabled smart healthcare system with public verifiability," *IEEE Internet Things J.*, vol. 7, no. 10, pp. 10650–10659, Oct. 2020.

[4] C. Huang, A. Zappone, and G. C. Alexandropoulos *et al*, "Reconfigurable intelligent surfaces for energy efficiency in wireless communication," *IEEE Trans. Wireless Commun.*, vol. 18, no. 8, pp. 4157-4170, Aug. 2019.

[5] Z. Chu, W. Hao, and P. Xiao *et al*, "Intelligent reflecting surface aided multi-antenna secure transmission," *IEEE Wireless Commun. Lett.*, vol. 9, no. 1, pp. 108-112, Jan. 2020.

[6] Q. Wang, F. Zhou, and R. Q. Hu *et al*, "Energy efficient robust beamforming and cooperative jamming design for IRS-assisted MISO networks," *IEEE Trans. Wireless Commun.*, vol. 20, no. 4, pp. 2592-2607, Apr. 2021.

[7] X. Mu, Y. Liu, and L. Guo *et al*, "Simultaneously transmitting and reflecting (STAR) RIS aided wireless communications," *IEEE Trans. Wireless Commun.*, 2021, early access, doi: 10.1109/TWC.2021.3118225.

[8] J. Xu, Y. Liu, and X. Mu *et al*, "STAR-RISs: Simultaneous transmitting and reflecting reconfigurable intelligent surfaces," *IEEE Commun. Lett.*, 2021, early access, doi: 10.1109/LCOMM.2021.3082214.

[9] G. Zhou, C. Pan, and H. Ren *et al*, "A framework of robust transmission design for IRS-aided MISO communications with imperfect cascaded channels," *IEEE Trans. Signal Process.*, vol. 68, pp. 5092-5106, Jan. 2020.

[10] Z.-Q. Luo, J. F. Sturm, and S. Zhang, "Multivariate nonnegative quadratic mappings," *SIAM J. Optim.*, vol. 14, no. 4, pp. 1140-1162, Jan. 2004.

[11] S. Boyd and L. Vandenberghe, *Convex Optimization. Cambridge*, U.K.: Cambridge Univ. Press, 2004.

[12] I. R. Petersen, "A stabilization algorithm for a class of uncertain linear systems," *Syst. Contr. Lett.*, no. 8, pp. 351-357, Jan. 1987.